

Homogenous Pd-Catalyzed Asymmetric Hydrogenation of Unprotected Indoles: Scope and Mechanistic Studies

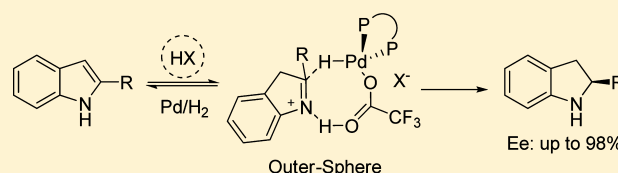
Ying Duan,^{‡,†} Lu Li,^{#,†} Mu-Wang Chen,[‡] Chang-Bin Yu,[‡] Hong-Jun Fan,^{*,‡} and Yong-Gui Zhou^{*,‡}

[‡]State Key Laboratory of Molecular Reaction Dynamics, Dalian Institute of Chemical Physics, Chinese Academy of Sciences, Dalian 116023, China

[#]State Key Laboratory of Fine Chemicals, Institute of Coal Chemical Engineering, School of Chemical Engineering, Dalian University of Technology, Dalian 116024, China

Supporting Information

ABSTRACT: An efficient palladium-catalyzed asymmetric hydrogenation of a variety of unprotected indoles has been developed that gives up to 98% ee using a strong Brønsted acid as the activator. This methodology was applied in the facile synthesis of biologically active products containing a chiral indoline skeleton. The mechanism of Pd-catalyzed asymmetric hydrogenation was investigated as well. Isotope-labeling reactions and ESI-HRMS proved that an iminium salt formed by protonation of the C=C bond of indoles was the significant intermediate in this reaction.



The important proposed active catalytic Pd–H species was observed with ¹H NMR spectroscopy. It was found that proton exchange between the Pd–H active species and solvent trifluoroethanol (TFE) did not occur, although this proton exchange had been previously observed between metal hydrides and alcoholic solvents. Density functional theory calculations were also carried out to give further insight into the mechanism of Pd-catalyzed asymmetric hydrogenation of indoles. This combination of experimental and theoretical studies suggests that Pd-catalyzed hydrogenation goes through a stepwise outer-sphere and ionic hydrogenation mechanism. The activation of hydrogen gas is a heterolytic process assisted by trifluoroacetate of Pd complex via a six-membered-ring transition state. The reaction proceeds well in polar solvent TFE owing to its ability to stabilize the ionic intermediates in the Pd–H generation step. The strong Brønsted acid activator can remarkably decrease the energy barrier for both Pd–H generation and hydrogenation. The high enantioselectivity arises from a hydrogen-bonding interaction between N–H of the iminium salt and oxygen of the coordinated trifluoroacetate in the eight-membered-ring transition state for hydride transfer, while the active chiral Pd complex is a typical bifunctional catalyst, effecting both the hydrogenation and hydrogen-bonding interaction between the iminium salt and the coordinated trifluoroacetate of Pd complex. Notably, the Pd-catalyzed asymmetric hydrogenation is relatively tolerant to oxygen, acid, and water.

INTRODUCTION

Chiral indolines are a significant class of alkaloids found in numerous bioactive compounds, such as pharmaceuticals, herbicides, and insecticides.¹ These privileged motifs are key building blocks in the discovery of drugs. Although the demand for enantiomerically pure indolines is growing as time goes on, the methods to reach them are still limited. Because indoles have inherent stability and it is difficult to modify their aromatic properties, the journey from indoles to indolines has a long way to go. From the perspective of atom economy, asymmetric hydrogenation is the most direct and important way to achieve this process.² As a huge family of heteroaromatic compounds, indoles have been shown to have important applications in organic synthesis, but they exhibited inertness in asymmetric hydrogenation until 2000.

In 2000, Ito, Kuwano, and co-workers³ reported the first example of asymmetric hydrogenation of *N*-protected indoles using a Rh/Ph-TRAP complex as catalyst. Thereafter, Rh/Ph-TRAP⁴ and Ru/Ph-TRAP⁵ were found to be useful in asymmetric hydrogenation of indoles with an electron-withdrawing group on the nitrogen atom. The groups of Minnaard⁶

and Agbossou–Niedercorn⁷ then found that a complex of Rh and PinPhos or WalPhos as catalyst could also promote asymmetric hydrogenation of *N*-protected indoles. The Ir/N,P-ligand system was a desirable candidate as well, yet it gave barely satisfactory yields.⁸ There was virtually no development in the hydrogenation of simple indoles until our group introduced the strategy of Brønsted acid activation (Scheme 1).⁹ In that work, a powerful Pd catalyst system was selected due to its inertness to strong Brønsted acids. Subsequently, dehydration-triggered asymmetric hydrogenation¹⁰ and consecutive Brønsted acid/Pd-complex-promoted tandem reactions¹¹ were also reported. Moreover, 3-(toluenesulfonamidoalkyl)-indoles were synthesized and hydrogenated to form chiral indolines.^{12,13}

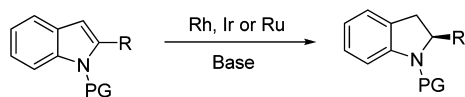
Chiral Pd-based catalysts have achieved great successes in asymmetric hydrogenation of a large range of substrates,¹⁴ such as activated imines,¹⁵ enamines,¹⁶ functional ketones,¹⁷ olefins,¹⁸ and also heteroaromatic compounds.^{9–12,19} However,

Received: February 26, 2014

Published: April 30, 2014

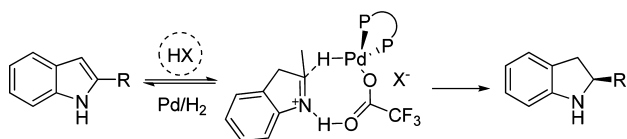
Scheme 1. Strong Brønsted Acid Activation Strategy for Asymmetric Hydrogenation of Unprotected Indoles

Previous Work: Asymmetric Hydrogenation of *N*-Protected Indoles



PG = Ts, Ac, Boc

This Work: Asymmetric Hydrogenation of *N*-Unprotected Indoles



there are also some issues to be noted in these reactions. First, trifluoroethanol (TFE) has always been the best solvent, but that was challenged in the hydrogenation of simple indoles and pyrroles. Second, the detailed mechanism of Pd-catalyzed asymmetric hydrogenation remains to be elucidated, in terms of the fashion of hydrogen gas activation or the dissociation of Pd catalyst from the product. This question is relatively unexplored, in contrast to Ir,²⁰ Ru,²¹ or Rh²²-catalyzed asymmetric hydrogenations. In this article, we extend the scope of Pd-catalyzed asymmetric hydrogenation of unprotected indoles and gain insight into the mechanism of Pd-catalyzed asymmetric hydrogenation by a combination of experimental and theoretical studies.

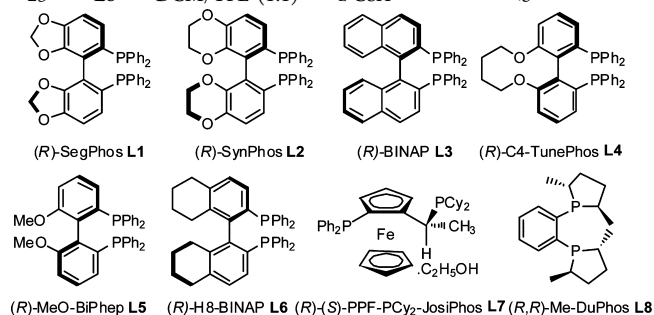
RESULTS AND DISCUSSION

Asymmetric Hydrogenation of Simple 2-Substituted Indoles.

2-Methylindole was chosen as the model substrate to assay the best reaction conditions for asymmetric hydrogenation, and Pd(OCOCF₃)₂/(*R*)-SegPhos complex was applied to begin the investigation. As shown in Table 1, hydrogenation does not occur in the absence of Brønsted acid (entry 1). To achieve full conversion and high enantioselectivity requires a stoichiometric amount of Brønsted acid to activate 2-methylindole. First, the effects of Brønsted acids on the reactivity and enantioselectivity were examined. Among the strong Brønsted acids, PhSO₃H, TsOH·H₂O, and *L*-camphorsulfonic acid (*L*-CSA) gave full conversions and moderate enantiomeric excess (ee) values (Table 1, entries 3, 4, and 6); *L*-CSA gave full conversion and the highest enantioselectivity (entry 6, 71% ee). In contrast, *D*-CSA with the opposite configuration gave product with 44% conversion and somewhat lower ee (entry 7, 66% ee). These varied activities and ee values may ascribed to the different matching ability of the chiral ligand and the two CSAs. However, with weak Brønsted acids, such as benzoic acid and salicylic acid, either low turnover or low enantioselectivity was observed. Therefore, it was concluded that *L*-CSA was the best activator to promote this asymmetric hydrogenation, on the basis of the data in Table 1. Second, the effect of solvent was evaluated, and it was found that solvent influenced both conversions and ee values dramatically (Table 1, entries 6, 10–13). Fortunately, the combination of equal volumes of DCM and TFE resulted in full conversion and higher ee (Table 1, entries 15 vs 14 and 16). Finally, examination of various bisphosphine ligands showed that (*R*)-H8-BINAP promoted the ee value to 91% (Table 1, entries 17–23). After screening a wide range of parameters for indole **1a**, we determined the optimized conditions: Pd(OCOCF₃)₂/(*R*)-H8-BINAP/*L*-CSA/rt/TFE:DCM = 1:1.

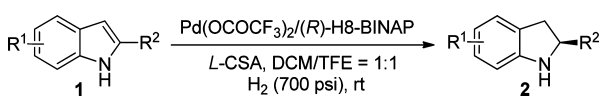
Table 1. Optimization of Conditions for Asymmetric Hydrogenation of 2-Substituted Indole **1a**^a

entry	ligand	solvent	acid	conv (%) ^b	ee (%) ^c
1	L1	TFE	–	<5	–
2	L1	TFE	TfOH	61	54 (R)
3	L1	TFE	PhSO ₃ H	>95	62 (R)
4	L1	TFE	TsOH·H ₂ O	>95	69 (R)
5	L1	TFE	TFA	>95	8 (R)
6	L1	TFE	<i>L</i> -CSA	>95	71 (R)
7	L1	TFE	<i>D</i> -CSA	44	66 (R)
8	L1	TFE	PhCO ₂ H	<5	25 (R)
9	L1	TFE	salicylic acid	35	4 (R)
10	L1	MeOH	<i>L</i> -CSA	19	40 (R)
11	L1	toluene	<i>L</i> -CSA	57	57 (R)
12	L1	THF	<i>L</i> -CSA	<5	–
13	L1	DCM	<i>L</i> -CSA	89	73 (R)
14	L1	DCM/TFE (2:1)	<i>L</i> -CSA	>95	82 (R)
15	L1	DCM/TFE (1:1)	<i>L</i> -CSA	>95	85 (R)
16	L1	DCM/TFE (1:2)	<i>L</i> -CSA	>95	80 (R)
17	L2	DCM/TFE (1:1)	<i>L</i> -CSA	>95	86 (R)
18	L3	DCM/TFE (1:1)	<i>L</i> -CSA	>95	81 (R)
19	L4	DCM/TFE (1:1)	<i>L</i> -CSA	>95	84 (R)
20	L5	DCM/TFE (1:1)	<i>L</i> -CSA	>95	84 (R)
21	L6	DCM/TFE (1:1)	<i>L</i> -CSA	>95	91 (R)
22	L7	DCM/TFE (1:1)	<i>L</i> -CSA	49	80 (R)
23	L8	DCM/TFE (1:1)	<i>L</i> -CSA	<5	–



^aConditions: indole **1a** (0.25 mmol), acid (0.25 mmol), Pd(OCOCF₃)₂ (2 mol%), ligand (2.4 mol%), solvent (3.0 mL), 24 h, rt. ^bDetermined by ¹H NMR. ^cDetermined by HPLC.

With the optimized conditions in hand, we investigated the range of substrates (Table 2). Those substrates bearing primary or secondary alkyl groups could all give excellent ee values and moderate to excellent yields. The length of 2-alkyl substituent as well as the size of the cyclic alkyl substituent had little effect on the enantioselectivities (Table 2, entries 1–5). 2-Phenethyl- and 2-benzylindole could also give prominent ee values, 93% and 95%, respectively (Table 2, entries 6 and 7). The steric effect of benzene ring bearing on benzyl displayed little concern with activities and enantioselectivities (Table 2, entries 8–11). γ -Ester group was tolerated and high ee was obtained with the slight modification of the reaction conditions (Table 2, entry 12), but hydroxyl was not so fortunate (Table 2, entry 13). However, the presence of group at C5 of indole, such as 5-fluoro and 5-methyl, decreased the ee values to 88% and 84%, respectively (Table 2, entries 14 and 15). Unfortunately, 2-carbalkoxy and 2-styryl group inhibited the reaction, and the

Table 2. Pd-Catalyzed Asymmetric Hydrogenation of 2-Substituted Indoles 1^a


entry	R ¹	R ²	yield (%) ^b	ee (%) ^c
1	H	Me	88 (2a)	91 (R)
2	H	<i>n</i> -Bu	82 (2b)	93 (R)
3	H	<i>n</i> -pentyl	89 (2c)	92 (R)
4	H	Cy	90 (2d)	95 (S)
5	H	cyclopentyl	85 (2e)	95 (S)
6	H	phenethyl	89 (2f)	93 (R)
7	H	Bn	99 (2g)	95 (R)
8	H	2-MeC ₆ H ₄ CH ₂	84 (2h)	94 (R)
9	H	3-MeC ₆ H ₄ CH ₂	95 (2i)	94 (R)
10	H	4-MeC ₆ H ₄ CH ₂	82 (2j)	93 (R)
11	H	1-naphthyl-CH ₂	78 (2k)	96 (R)
12 ^d	H	CH ₂ CH ₂ COOEt	98 (2l)	84 (R)
13	H	CH ₂ CH ₂ CH ₂ OH	<5	–
14	5-F	Me	84 (2m)	88 (R)
15	5-Me	Me	81 (2n)	84 (R)
16	H	COOEt	<5	–
17	H	styryl (<i>E</i>)	<5	–
18	H	CF ₃	<5	–
19	H	<i>t</i> -Bu	<5	–
20	H	Ph	<5	–

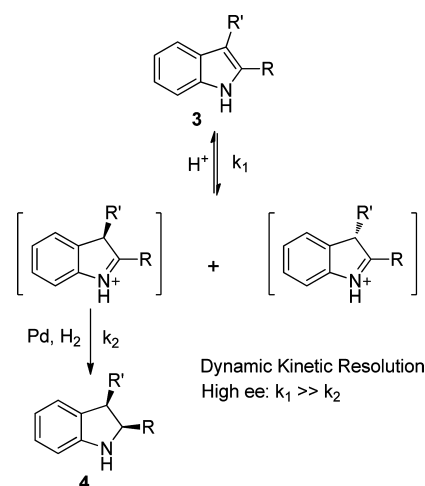
^aConditions: **1** (0.25 mmol), L-CSA (0.25 mmol), Pd(OCOCF₃)₂ (2 mol%), (R)-H8-BINAP (2.4 mol%), DCM/TFE (3 mL, 1:1), 24 h, rt. ^bIsolated yield. ^cDetermined by HPLC. ^d50 °C.

double bond of the styryl group was intact (Table 2, entries 16 and 17). Meanwhile, sterically more demanding groups (*tert*-butyl) and electron-withdrawing groups (trifluoromethyl group) were problematic with low activity (Table 2, entries 18 and 19). Disappointingly, almost no reaction was observed when 2-phenylindole was subjected to the standard conditions (Table 2, entry 20).

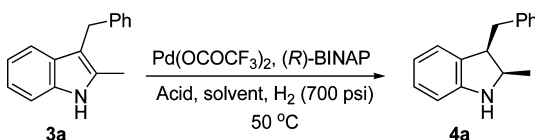
Asymmetric Hydrogenation of Simple 2,3-Disubstituted Indoles. Encouraged by successful asymmetric hydrogenation of unprotected 2-substituted indoles, we next turned our attention to asymmetric hydrogenation of 2,3-disubstituted indoles. Unlike the results with the simple 2-substituted indoles, two contiguous chiral centers will be obtained in the hydrogenation of 2,3-disubstituted indoles. These two chiral carbons are produced in different steps: asymmetric protonation and asymmetric hydrogenation. Initially, the chiral center at the 3-position is generated from protonation of indole **3**. Subsequently, selective hydrogenation of one of the isomers gives the hydrogenation product **4** (Scheme 2). Indeed, a classical dynamic kinetic asymmetric transformation process is involved in this reaction.

Accordingly, to obtain enantiomerically pure products, the protonation step should be much faster than the hydrogenation step ($k_1 \gg k_2$). A higher reaction temperature should accelerate the protonation step, and a lower pressure of hydrogen gas should decrease the rate of hydrogenation of the iminium intermediate. Based on the theoretical analysis, a higher temperature as well as a lower pressure of hydrogen gas might guarantee the success of this process.

Thus, the reaction temperature of hydrogenation was increased to 50 °C for further reaction optimization. Initial solvent screening showed that the mixed solvent DCM/TFE

Scheme 2. Asymmetric Hydrogenation of 2,3-Disubstituted Indoles **3** via a Dynamic Kinetic Resolution Process

(2:1) gave better results than the others (Table 3, entry 3 vs entries 1 and 2), yielding only the *cis*-2,3-disubstituted indoline

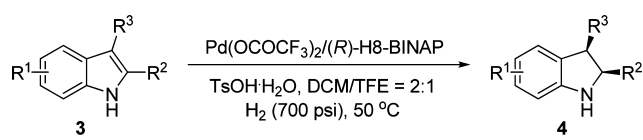
Table 3. Optimization for Asymmetric Hydrogenation of 2,3-Disubstituted Indole **3a**^a


entry	solvent	acid	yield (%) ^b	ee (%) ^c
1	DCM/TFE (1:2)	TsOH·H ₂ O	77	86
2	DCM/TFE (1:1)	TsOH·H ₂ O	98	87
3	DCM/TFE (2:1)	TsOH·H ₂ O	84	88
4	DCM/TFE (2:1)	L-CSA	95	85
5	DCM/TFE (2:1)	D-CSA	85	86
6	DCM/TFE (2:1)	MeSO ₃ H	75	81
7	DCM/TFE (2:1)	EtSO ₃ H	80	83
8 ^d	DCM/TFE (2:1)	TsOH·H ₂ O	91	93

^aConditions: indole **3a** (0.25 mmol), acid (0.25 mmol), Pd(OCOCF₃)₂ (2 mol%), (R)-BINAP (2.4 mol%), solvent (3.0 mL), 24 h, 50 °C. ^bIsolated yield. ^cDetermined by HPLC. ^d(R)-H8-BINAP was used as the ligand.

isomer. A survey of sulfonic acids indicated that *p*-toluenesulfonic acid (TsOH·H₂O) was the best choice (Table 3, entry 3 vs entries 4–7). The ee value was enhanced to 93% (Table 3, entry 8) when asymmetric hydrogenation was performed with (R)-H8-BINAP as ligand. Therefore, the optimized reaction conditions are as follows: Pd(OCOCF₃)₂/(R)-H8-BINAP/TsOH·H₂O/DCM:TFE = 2:1 at 50 °C.

Under the optimized conditions, a variety of 2,3-disubstituted indoles were subjected to asymmetric hydrogenation, and excellent enantioselectivities and diastereoselectivities were obtained (Table 4). 3-Benzyl-substituted indoles were slightly inferior to 3-alkyl-substituted indoles in terms of ee for this asymmetric hydrogenation (Table 4, entries 1–3 vs entries 4 and 5). The introduction of electron-donating and electron-withdrawing groups on the phenyl ring of 3-benzyl was found to not affect the reaction significantly (Table 4, entry 2 vs entry 3). To ensure the high enantioselectivity of indolines **4**, a slight modification was made, such as reducing the hydrogen pressure

Table 4. Asymmetric Hydrogenation of 2,3-Disubstituted Indoles 3^a


entry	R ¹	R ² /R ³	yield (%) ^b	ee (%) ^c
1	H	Me/Bn	93 (4a)	91
2	H	Me/4-MeOC ₆ H ₄ CH ₂	94 (4b)	91
3	H	Me/4-FC ₆ H ₄ CH ₂	97 (4c)	91
4	H	Me/CyCH ₂	81 (4d)	94
5	H	Me/ <i>i</i> -PrCH ₂	89 (4e)	94
6	H	phenethyl/Bn	93 (4f)	94
7 ^d	H	-(CH ₂) ₄ -	91 (4g)	91 (R,R)
8 ^d	H	-(CH ₂) ₅ -	96 (4h)	90 (R,R)
9 ^{d,e}	H	Me/Me	84 (4i)	92 (R,R)
10	5-F	Me/Bn	93 (4j)	87
11	5-F	Me/CyCH ₂	92 (4k)	92
12	7-Me	Me/Bn	95 (4l)	97
13	7-Me	Me/CyCH ₂	87 (4m)	96
14	7-Me	Me/2-MeC ₆ H ₄ CH ₂	82 (4n)	98
15	7-Me	Me/3-MeC ₆ H ₄ CH ₂	98 (4o)	97
16	7-Me	Me/4-MeC ₆ H ₄ CH ₂	87 (4p)	97
17 ^{d,e}	7-Me	-(CH ₂) ₄ -	83 (4q)	96 (R,R)
18	H	Me/CO ₂ Et	<5	-

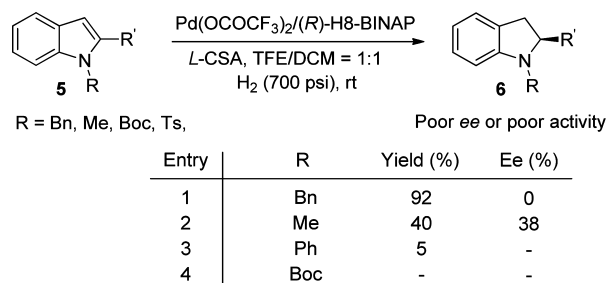
^aConditions: indole 3 (0.25 mmol), TsOH·H₂O (0.25 mmol), Pd(OCOCF₃)₂ (2 mol%), (R)-H8-BINAP (2.4 mol%), DCM/TFE (3.0 mL, 2:1), 24 h, 50 °C. ^bIsolated yield. ^cDetermined by HPLC.

^dUsing L-CSA and solvent (DCM/TFE 1:1) at rt. ^e50 °C and H₂ (300 psi).

(Table 4, entries 9 and 17). We found that ring-fused substrates could also give satisfying results (Table 4, entries 7–9 and 17), and indoles bearing a 5-F substituent displayed slightly lower ee than other indoles (Table 4, entries 10 and 11). 7-Methyl-substituted 2,3-disubstituted indoles showed remarkable enantioselectivities (96–98% ee, Table 4, entries 12–17). Unfortunately, 3-carbalkoxy-2-methylindole 3r could not be hydrogenated under the standard conditions (Table 4, entry 18).

Asymmetric Hydrogenation of *N*-Protected Indoles.

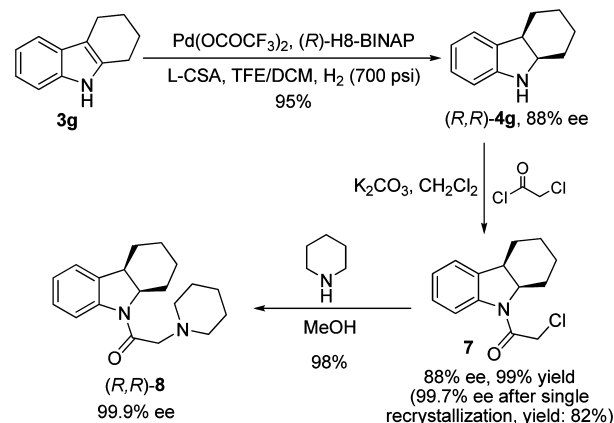
N-Protected indoles were also subjected to hydrogenation under the above standard conditions (Scheme 3). Unfortunately, it was found that these substrates were not good partners for Pd catalyst system. The low enantioselectivity might be due to that fact that the protecting groups on the *N*-atom prevent the generation of an iminium intermediate and/or inhibit hydrogen-bonding interaction with the trifluoroac-

Scheme 3. Asymmetric Hydrogenation of *N*-Protected Indoles

tate coordinated on the Pd catalyst. These two points are crucial for Pd-catalyzed asymmetric hydrogenation of unprotected indoles (for details, see the Mechanistic Study section).

Product Elaboration. To demonstrate the utility of Pd-catalyzed asymmetric hydrogenation of the unprotected indoles, a direct and efficient method was developed to synthesize the enantiopure indoline skeleton derivative 8, a neuroleptic agent in many types of antidepressants.²³ As shown in Scheme 4, asymmetric hydrogenation of 2,3-disubstituted

Scheme 4. Synthesis of Biologically Active Product 8

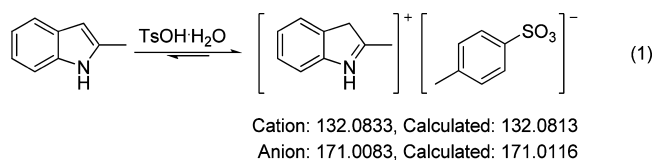


indole 3g gave the key intermediate hexahydrocarbazole 4g with 88% ee. Subsequent protection with 2-chloroacetyl chloride and a simple recrystallization afforded the intermediate 7 with 99% ee. Finally, *N*-alkylation gave the biologically active compound 8 in high overall yields and up to 99.9% ee.

MECHANISTIC STUDY

Iminium Intermediate. Iminium and vinylogous iminium have been found to be significant intermediates in numerous organic reactions,²⁴ and they are also crucial for the success of the asymmetric hydrogenation of unprotected indoles.

Further confirmation of the presence of the iminium in the hydrogenation reaction is required; therefore, iminium salt was conveniently prepared with the equivalent 2-methylindole and TsOH·H₂O in CDCl₃ after stirring 5 min at room temperature. ¹H NMR investigation indicated that the signal of the hydrogen at the 3-position became broad and shifted upfield, and the *N*-H peak disappeared rapidly. When TsOH·H₂O was exchanged with D₂O before being applied to this system, all the peaks from the ¹H NMR study in CDCl₃ remained the same as before, except for the partial disappearance of the 3-H of iminium (Figure 1). Subsequent electrospray ionization mass spectroscopic analysis of a similar solution showed peaks at *m/z*⁺ 132.0833 and *m/z*⁻ 171.0083, which agreed with the ion pair of the iminium intermediate (eq 1). In this way, the iminium salt generated before hydrogenation was identified.



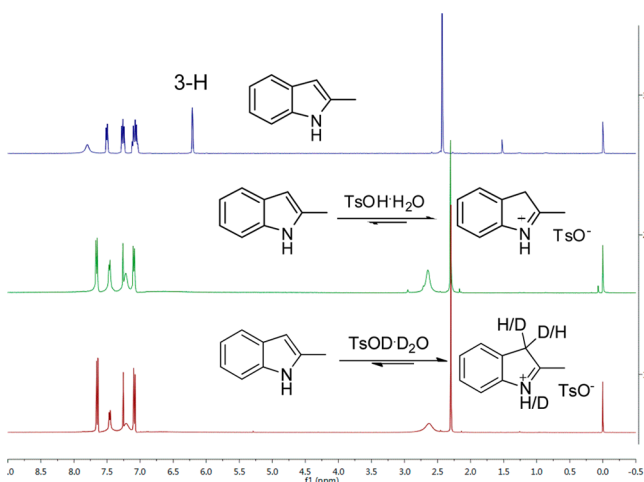
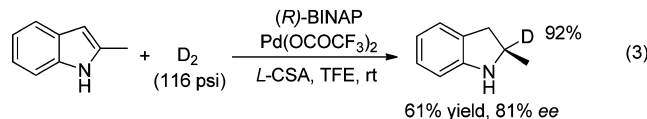
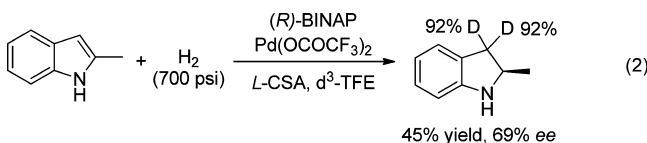


Figure 1. ^1H NMR study of $\text{TsOH}\cdot\text{H}_2\text{O}$ or $\text{TsOD}\cdot\text{D}_2\text{O}$ as well as 2-methylindole in CDCl_3 .

Isotopic labeling experiments using deuterated solvent and deuterium gas also affirmed the above conclusion (eqs 2 and 3).

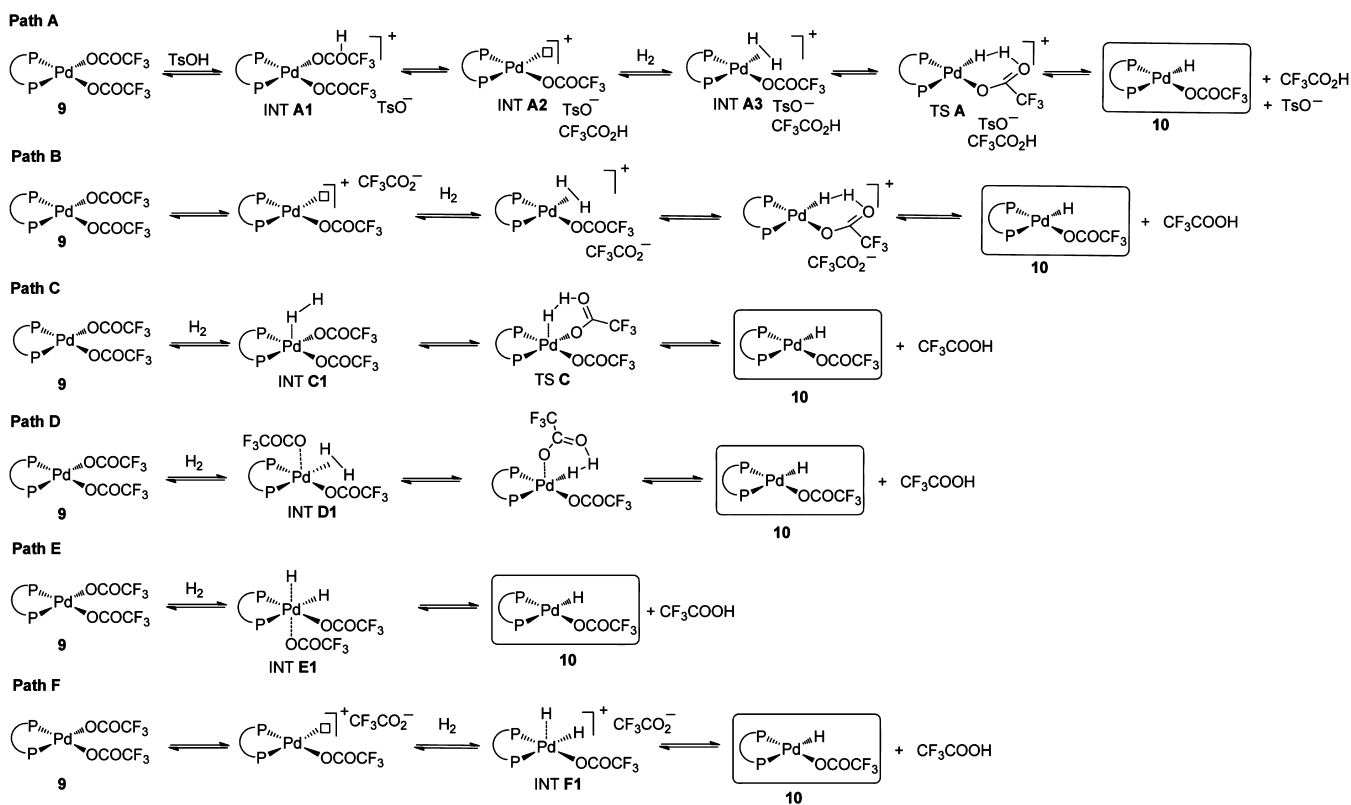


The first step was generation of the iminium intermediate, and then this active iminium intermediate was hydrogenated to afford the desired product. When the asymmetric hydrogenation was run in deuterated TFE, ^1H NMR analysis of the crude products showed that two deuterium atoms were incorporated at the 3-position of 2-methylindoline (eq 2), which suggested a fast, reversible process of protonation and deprotonation. Thus, two deuterium atoms were incorporated at the 3-position before hydrogenation. When 2-methylindole was subjected to hydrogenation with D_2 , 2-deuterio-2-methylindoline with 92% incorporation was obtained without deuterium at the 3-position (eq 3). The above experimental results suggested that the simple unprotected indoles can be activated by a Brønsted acid to form iminium *in situ*, which can then be hydrogenated by the chiral Pd catalyst.

Active Pd Hydride Species. Metal hydride active species have been involved not only in hydrogenation but also in many other organic reactions as the key intermediate. However, several factors impede the thorough study of the metal hydride intermediates.²⁵ Generally, the metal hydrides are generated in the reaction in only trace amounts, and the metal hydrides are unstable in many conditions. Therefore, it is challenging to isolate them and determine their conformations or properties.²⁶ Given the importance of metal hydrides in such reactions, especially in hydrogenation reactions, here we present the most likely paths to generate Pd–H in the Pd-catalyzed asymmetric hydrogenation, based on our experience.

As can be seen from Scheme 5 and Figure 2, in path A, first, protonation of one CF_3COO^- ligand by strong acid TsOH gives INT A1, and then the CF_3COOH ligand is detached from the Pd catalyst to generate an unoccupied site, INT A2. H_2 combines with this active center (INT A3) and is activated with

Scheme 5. Proposed Pathways for Reaction of Hydrogen Gas and Pd Catalyst To Generate Pd–H Species



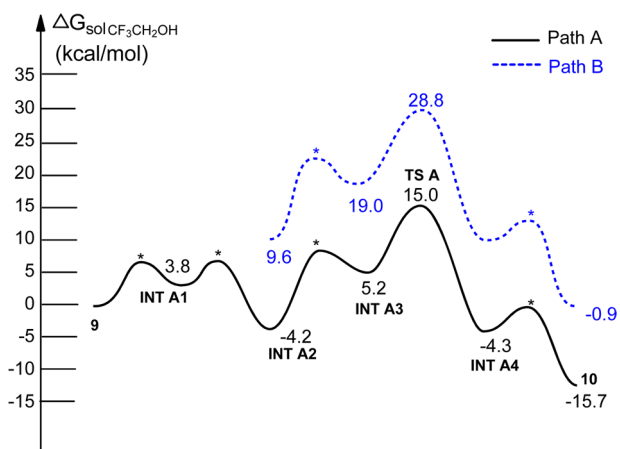


Figure 2. Computed reaction energy profiles for path A (with the help of TsOH) and path B (strong acid is not involved) to generate palladium hydride in TFE. Relative energies in kcal/mol are given.

assistance from Pd and the coordinated CF_3COO^- ligand (TS A). The last step is the ligand exchange (or proton exchange) between CF_3COO^- and the coordinated CF_3COOH (INT A4) to offer the Pd–H species 10. In path B, one CF_3COO^- ligand is directly detached from the Pd catalyst to generate an unoccupied site, INT A2. The following steps are the same as in path A. In path C, H_2 coordinates to Pd catalyst first (INT C1) and then is activated by Pd and a CF_3COO^- ligand. Pd–H species 10 is generated with the remaining coordinated CF_3COOH . Path D is similar to path C, except that CF_3COO^- is on the apical position in INT D1, while H_2 is on the apical position in INT C1. H_2 is activated by Pd and a CF_3COO^- ligand. In path E, H_2 is activated by the Pd catalyst through oxidative addition, followed by reductive elimination of CF_3COOH to generate the Pd–H species 10. In path F, the first step is similar to that in path B, but H_2 is activated by the unsaturated Pd catalyst center through oxidative addition. Finally, the Pd–H species is generated after release of CF_3COOH . Paths A, B, and F are ionic pathways, while paths C, D, and E are not. Paths C and D may suffer due to the five-coordinated TS C, INT C1, and INT D1, which are not common for transition metals with d^8 configuration. Paths E and F may suffer due to the oxidative addition, since H_2 may not be able to oxidize Pd(II) to Pd(IV).

DFT calculations were carried out to elucidate which is the most facile path,²⁷ using TFE as the solvent (B3LYP; for details, see Supporting Information). First, the rate-determining barrier of path C is 32.9 kcal/mol. The energies of INT D1 (30.3 kcal/mol), INT E1 (46.6 kcal/mol), and INT F1 (44.8 kcal/mol) were found to be too high. Therefore, paths C–F were ruled out. All rate-determining barriers mentioned in this section were relative to the most stable structure prior to the rate-determining step, which means INT A2 for path A and reactant Pd catalyst 9 for all other paths. The reaction profiles of paths A and B are shown in Figure 2. We found that path A is preferred, with the rate-determining barrier of 19.2 kcal/mol. Protonation of the Pd catalyst by TsOH requires 3.8 kcal/mol. Releasing the CF_3COOH ligand gains 8.0 kcal/mol and offers an unoccupied site on Pd ion, which facilitates the H_2 coordination and activation. The H_2 activation step is the rate-determining step. The barrier of path B is higher than that of path A by 13.8 kcal/mol ($\Delta G_{\text{TS B}} - \Delta G_{\text{TS A}}$), which arises from the thermodynamic stability difference between TsO^- and

CF_3COO^- . The transition states marked with * in Figure 2 are for the ligand coordination or detachment steps. Harvey has recently suggested that such processes correspond to diffusion control,²⁸ with free energy barriers of ca. 4.5 kcal/mol, and are not expected to be competitive with the rate-determining barriers. The key transition state TS A is shown in Figure 3. It is

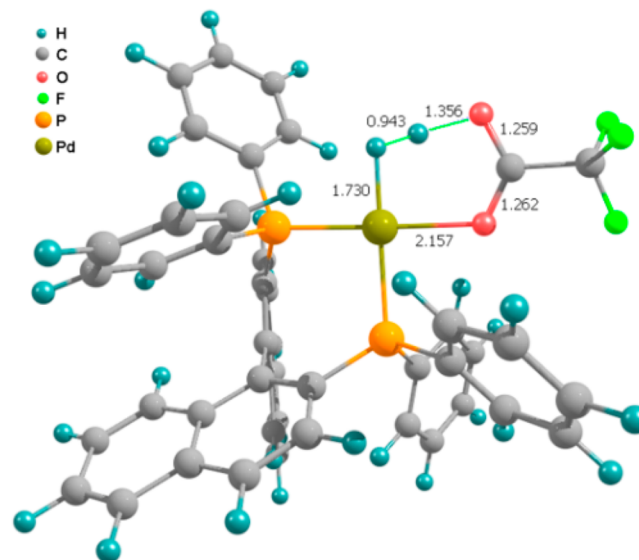


Figure 3. Computed structure of TS A. Bond lengths are given in Å.

an earlier transition state ($\text{H}-\text{H} = 0.94 \text{ \AA}$ in TS A) with square-planar structure as one would expect for d^8 transition metals. The transition state (TS C) of the non-ionic path C is shown in Figure 4. It has a square-pyramid structure, with the weakly coordinated CF_3COO^- ($\text{Pd}-\text{O} = 2.52 \text{ \AA}$) on the apical position.

Toward lifting the veil of active Pd–H, ^1H NMR was at the top of our list. As to the equilibrium between Pd catalyst and Pd–H species (Scheme 6), the low concentration of Pd–H met our expectation, but also made it difficult to study. Under

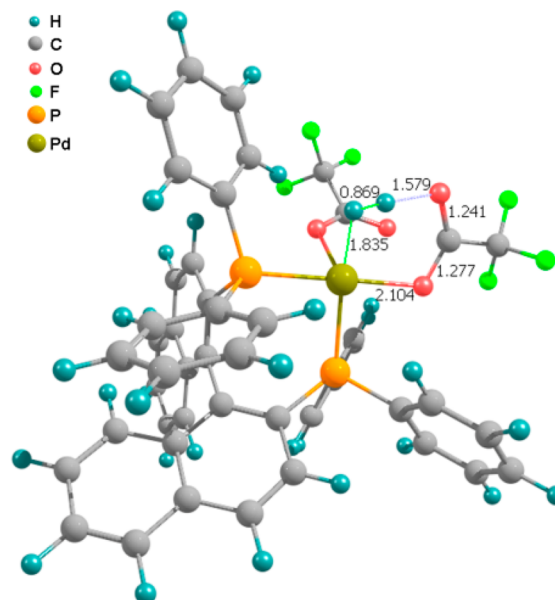
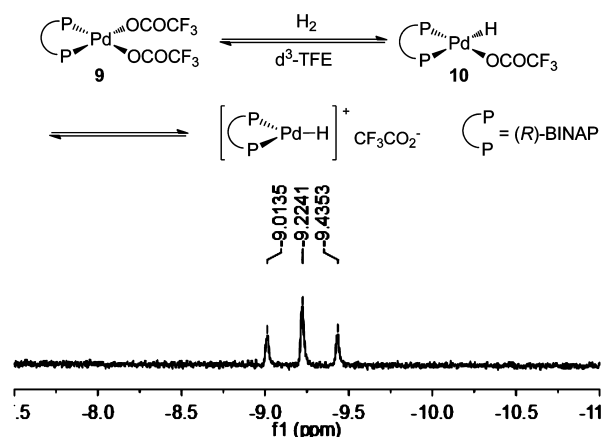
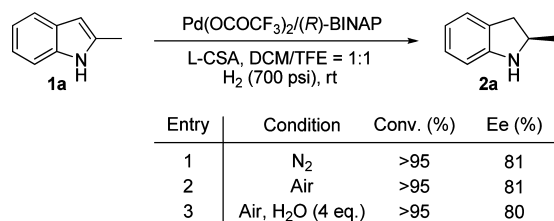


Figure 4. Computed structure of TS C. Bond lengths are given in Å.

Scheme 6. Generation and ¹H NMR Spectrum of Pd–H

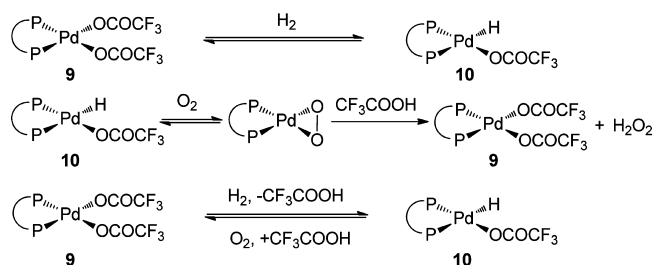
rigidly controlled conditions, fortunately, some proofs were obtained. A diagnostic virtual triplet in the ¹H NMR spectrum at -9.22 ppm ($J = 84.4$ Hz) (Scheme 6) and the chemical shift were consistent with most of the metal hydrides reported.²⁶ Since the coupling constant was between those of hydrogen coupling with *cis*-phosphorus ($J = 5\text{--}16$ Hz) and hydrogen coupling with *trans*-phosphorus ($J \approx 160$ Hz), it was inferred that the hydrogen in Pd–H couples with phosphorus with an angle between the *cis* and *trans* positions. This could be ascribed to equilibrium between the reversible reductive elimination of TFA and some other intermediates (Scheme 6). Also, an interesting phenomenon was observed in studying Pd–H species. When the chiral palladium catalyst [Pd(OCOCF₃)₂](*R*)-BINAP was put in the TFE, the solution was yellow. After being subjected to hydrogen gas, the solution turned from yellow to red, and deep red about 15 min later. This color does not fade over time or upon subjecting the solution to oxygen.

Robustness of Pd Catalyst to Air and Water. In the process of running experiments, we found that the chiral Pd-catalyzed asymmetric hydrogenation is relatively robust to air, acid, and water. In order to study this issue further, several controlled experiments were designed, as shown in Scheme 7

Scheme 7. Controlled Experiments on the Influence of Air and H₂O

(Table 1, entry 18 is equal to Scheme 7, entry 1). First, we performed the hydrogenation in the atmosphere without the Schlenk technique (Scheme 7, entry 2); i.e., the catalyst was prepared in the air and the substrate, Brønsted acid, solvent, and the catalyst were also mixed in the air. The experimental results confirmed our deduction that the hydrogenation went on well with similar activity and enantioselectivity (Scheme 7, entry 1 vs entry 2). Second, we added water to the reaction solution (Scheme 7, entry 3). No difference was noticed until 4 equiv of water relative to substrate was added to the reaction

(Scheme 7, entry 1 vs entry 3). The results of these experiments suggest that chiral the Pd catalyst has a relatively impassive behavior to air and water. To explain this, we proposed that the Pd–H generated from Pd(OCOCF₃)₂ under H₂ atmosphere could be oxidized to hydrogen peroxide or water and Pd(II) by oxygen in the presence of trifluoroacetic acid (Scheme 8), which has been reported by Sigman and

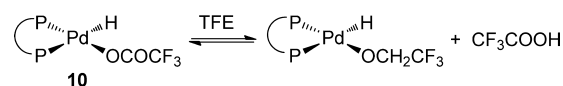
Scheme 8. Proposed Reasons for the Stability of Pd Catalyst to O₂

Stahl.^{25f,g,i-k} But it was not ruled out that the Pd–H complex is simply unreactive toward O₂. Actually, the formed Pd(II) species is our hydrogenation catalyst precursor, so the Pd–H can be regenerated. Therefore, the Pd catalyst is relatively insensitive to air, acid, and water.

Roles of Solvent Trifluoroethanol. Fluorinated alcohols, especially hexafluoroisopropanol (HFIP) and TFE, are used as solvents, cosolvents, and additives in many reactions, given their unique properties.²⁹ These properties, which made fluorinated alcohols a range of robust solvents, were usually considered to be high hydrogen bond donor ability, low nucleophilicity, high ionizing power, ability to solvate water, and so on. TFE, as one of the inexpensive fluorinated alcohols, has been commonly applied in synthetic chemistry.

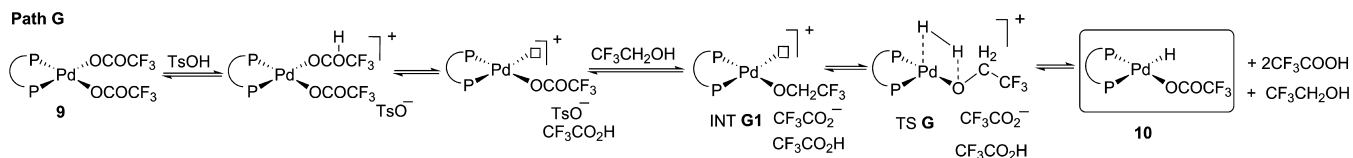
Recently, asymmetric hydrogenation has gained much interest because of its superb ability to construct chiral compounds. Our group contributed many examples to this thriving area. When we reviewed these hydrogenation reactions, an interesting phenomenon was noticed: excellent enantioselectivity and high activity are generally obtained in TFE in the Pd-catalyzed asymmetric hydrogenations. According to the literature and our experiences, two conclusions might be drawn: (1) TFE participates in the formation of some key intermediates,³⁰ or (2) TFE stabilizes these intermediates. As can be seen from Scheme 9, TFE participated in the exchange

Scheme 9. Exchange of the Counterion of Pd–H Complex and TFE



of the counterion of the Pd catalyst before or after the formation of Pd–H complex. Since CF₃CH₂O[−] is more nucleophilic than CF₃COO[−], this exchange seemed reasonable. But when we subjected the Pd catalyst to H₂ in TFE, followed by *in situ* IR, we found there is barely a peak at 1790 cm^{−1}, which is the characteristic peak of the carbonyl group of CF₃COOH.

The role of TFE has also been studied theoretically. First we studied whether TFE was involved in the reaction directly by replacing one CF₃COO[−] with CF₃CH₂O[−]. We only considered

Scheme 10. Possible TFE-Participating Pathway for Reaction of H₂ and Pd Catalyst To Generate Pd–H Species

path A because it is much more facile than the other paths. The new path is path G, as shown in Scheme 10. Replacing CF₃COO[−] with CF₃CH₂O[−] was found to be endothermic ($\Delta G = 7.8$ kcal/mol), which is consistent with the fact that CF₃COOH has not been detected experimentally. The rate-determining barrier (relative to INT A2, which is the most stable structure prior to the rate-determining step) is calculated to be 29.9 kcal/mol, higher than that of the corresponding non-TFE-participating path by more than 10 kcal/mol. Therefore, the theoretical results do not support that TFE participates in the Pd–H formation reaction directly.

Since we ruled out the TFE-participating paths, we began to accept the hypothesis that TFE stabilizes some key intermediates or transition states. This could be true since TFE is a highly polar solvent ($\epsilon = 26.5$) which is able to stabilize the ions in ionic paths such as path A, and it is inevitable that the barrier of path A is higher in a less polar solvent. To test this hypothesis, we got the reaction profiles for path A in CH₂Cl₂ ($\epsilon = 8.93$) for comparison (Figure 5). As

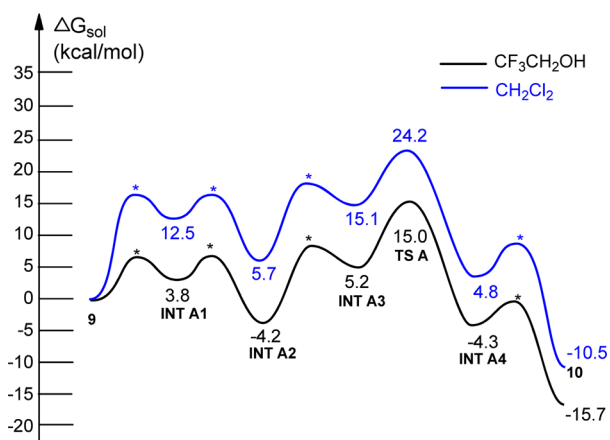


Figure 5. Computed reaction energy profiles for path A to generate palladium hydride in TFE and CH₂Cl₂. Relative free energies in kcal/mol are given.

expected, we found that in CH₂Cl₂ the rate-determining barrier of path A is 24.2 kcal/mol (relative to Pd catalyst 9), which is 9.2 kcal/mol higher than in TFE ($\Delta G_{\text{CH}_2\text{Cl}_2}^{\text{TSA}} - \Delta G_{\text{CF}_3\text{CH}_2\text{OH}}^{\text{TSA}}$). The ΔG of all other ionic intermediates also increases by 8–10 kcal/mol. On the basis of these calculations, we proposed that the unique properties of TFE and other fluorinated alcohols stem from their high polarity, which is able to stabilize the ionic intermediates during the catalytic reaction. Generally, the heterolytic splitting of a bond is very difficult and is usually facilitated by the strong solvation effect of the ions. For path A, the barrier is 89.4 kcal/mol in the gas phase, 24.2 kcal/mol in CH₂Cl₂, and 19.2 kcal/mol in TFE, which makes it facile under room temperature and high H₂ pressure.

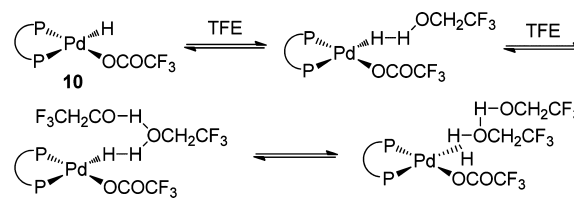
As a strong hydrogen bond donor,^{15a,31} the hydrogen atom of TFE can interact with the Pd–H (Scheme 11). This

Scheme 11. Possible Interaction of the TFE and Pd–H Species



phenomenon was also observed in many other metal hydride species, such as Ru–H and Ni–H.^{31a,c,32} It is reported that Ru–H and Ni–H could exchange proton with alcohol solvent (Scheme 12), but this exchange was not observed in the indole hydrogenation because there was no deuterium on the 2-C when d₃-TFE was subjected to hydrogenation (see eq 2).

Scheme 12. Possible Proton Exchange of the TFE and Pd–H Species

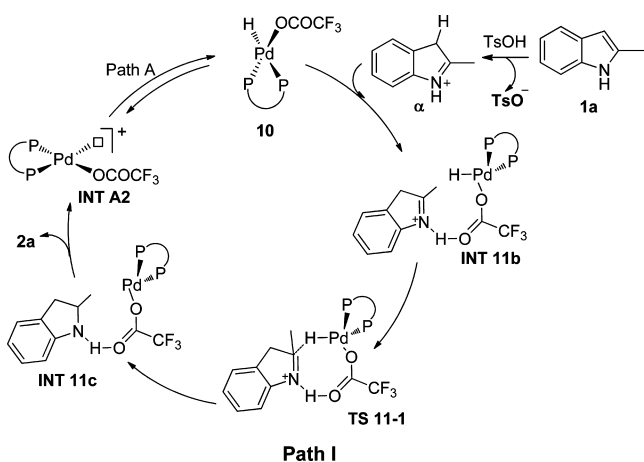


Proposed Catalytic Cycle of Indole Hydrogenation.

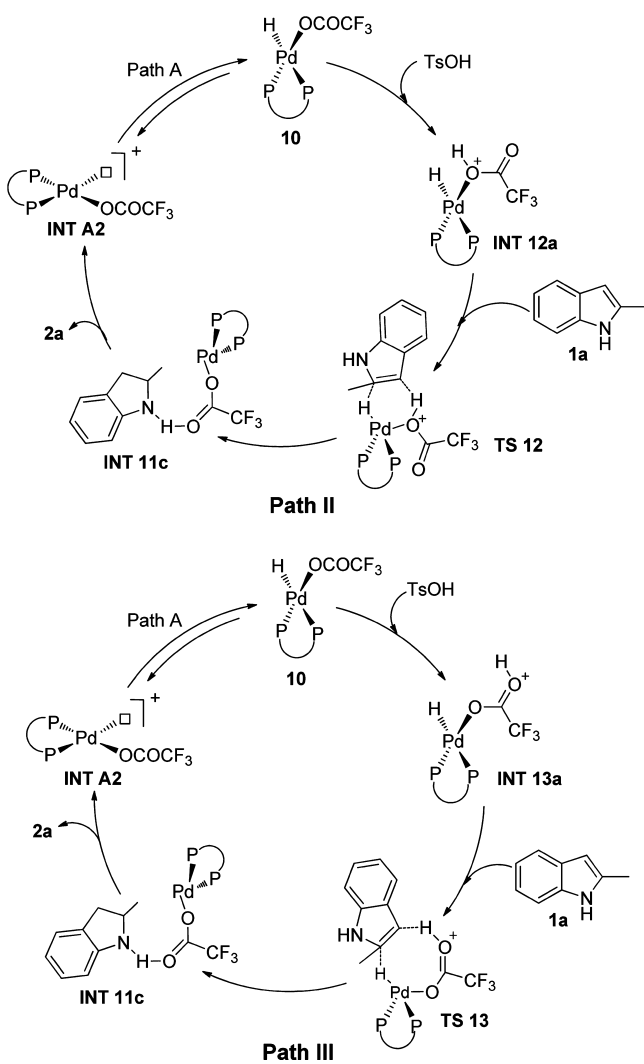
The catalytic mechanisms for hydrogenation reactions can be classified as (i) inner-sphere or outer-sphere mechanisms on the basis of the interaction between substrate and catalyst, (ii) ionic and non-ionic mechanisms according to the charge separation in the intermediates and transition states, as well as (iii) stepwise and associated mechanisms on the basis of the nature of the reaction pathway. In our search for the most plausible pathway for the indole hydrogenation, we have evaluated four paths including both inner-sphere and outer-sphere, ionic and non-ionic, stepwise and associated paths. As can be seen from Schemes 13–15 as well as Figures 6 and 7, path I (Scheme 13, Figure 7), first indole **1a** is protonated by TsOH to give iminium **α**, and then iminium **α** combines with Pd–H to generate INT **11b**. The next step is the hydride transfer from Pd–H to **α** to generate INT **11c**, which subsequently separates into product **2a** and INT **A2** and then follows path A to get the active catalyst Pd–H. This is an outer-sphere and ionic hydrogenation pathway. Alternatively, **1a** can also be protonated by CF₃COOH (generated in the Pd–H formation step) instead of TsOH.

Path II (Scheme 14), protonation of coordinated CF₃COO[−] by TsOH to give INT **12a**, followed by associated proton and hydride transfer to give **2a** and INT **A2**, involves a six-membered-ring transition state. This is an outer-sphere and non-ionic pathway. Path III is similar to path II except that CF₃COOH coordinates to Pd by C=O instead of the hydroxyl group. Accordingly, the associated hydrogenation has an eight-membered-ring transition state.

Scheme 13. Proposed Mechanism for the Asymmetric Hydrogenation of Indoles

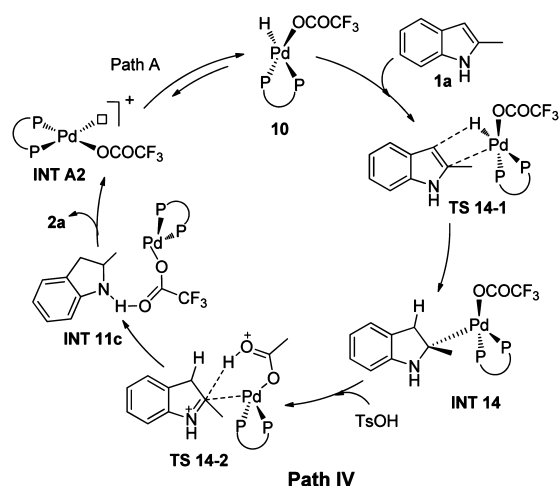


Scheme 14. Associated Pathways II and III for Indole Hydrogenation



In path IV (Scheme 15), Pd–H addition to the C=C bond of **1a** generates INT 14 first, and then the product **2a** and INT A2 are generated by proton transfer from CF₃COOH to

Scheme 15. Inner-Sphere Pathway for Indole Asymmetric Hydrogenation



the coordinated iminium. Path IV is an inner-sphere and non-ionic pathway.

All four pathways mentioned above have been studied computationally, and the reaction profiles in TFE are shown in Figure 6. Path I was found to be the most plausible one.

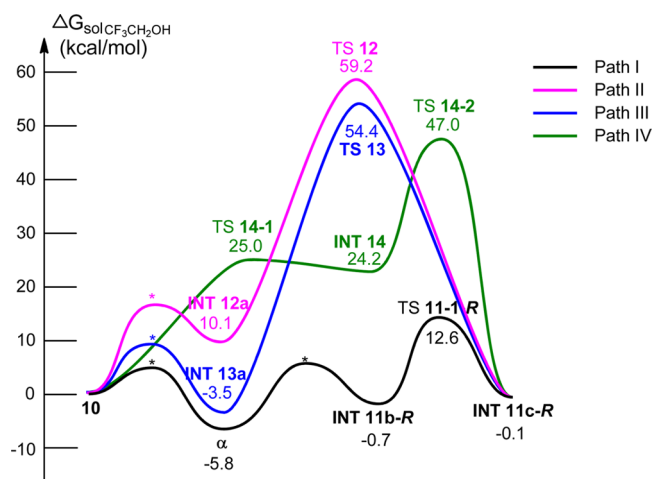


Figure 6. Computed reaction energy profiles for all paths to achieve asymmetric hydrogenation of unprotected indoles in TFE. Relative energies in kcal/mol are given.

Protonation of **1a** by TsOH is thermodynamically favorable ($\Delta G = -5.8$ kcal/mol), and the rate-determining step is the hydride transfer. As discussed above, all rate-determining barriers were relative to the most stable structure prior to the rate-determining step, which means α for path I, INT 13a for path III, and **10** for the other paths. The barriers for formation of (*R*)-**2a** and (*S*)-**2a** are 18.4 and 22.7 kcal/mol, respectively (Figure 7). The lower barrier for formation of (*R*)-**2a** is in good agreement with the high enantioselectivity observed experimentally. In CH₂Cl₂, both barriers are slightly lower (17.3 kcal/mol for (*R*)-**2a** and 21.6 kcal/mol for (*S*)-**2a**) than in TFE. This is because the protonation of **1a** by TsOH is already quite facile in CH₂Cl₂, while TFE overstabilizes the protonated intermediates and lowers its activity.

To confirm that the observed enantioselectivity is not method-dependent, the two key transition states leading to *R*

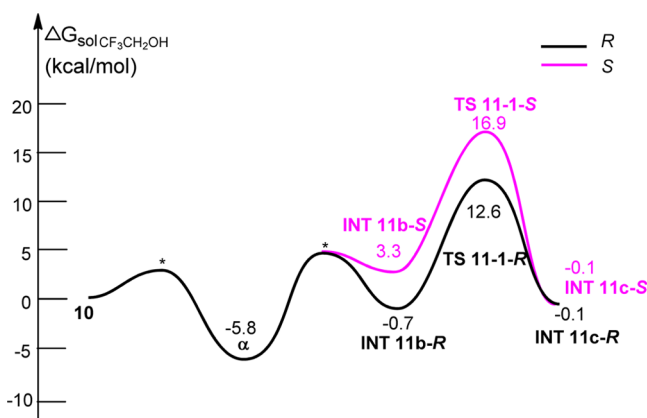


Figure 7. Computed reaction energy profiles for path I to achieve asymmetric hydrogenation of unprotected indoles in TFE. Relative free energies in kcal/mol are given.

and *S* isomers were reoptimized using the M06-2X functional. We found that TS-*R* is lower in energy (ΔG in $\text{CF}_3\text{CH}_2\text{OH}$) than TS-*S* by 3.5 kcal/mol, which is close to the 4.3 kcal/mol found by the B3LYP functional.

The indole hydrogenation described by this work does not occur without the presence of the strong acids such as *L*-CSA, TsOH, and MeSO_3H , etc., in contrast to the asymmetric hydrogenation of activated imines catalyzed by Pd complexes.^{15e} Using TsOH as the example, we have shown that the strong acid is involved in both the Pd–H generation and the hydrogenation. Without strong acid, indole can be protonated by the trifluoroacetic acid generated in the Pd–H formation step ($\Delta G = 8.0$ kcal/mol). The barriers for formation of (*R*)-**2a** and (*S*)-**2a** are 26.4 and 30.7 kcal/mol, respectively, both are much higher than those in path I.

Theoretically, a “three-point interaction model”³³ was usually used to explain the high enantioselectivity. According to this model, in order to have enantioselectivity, there must be at least three interactions between the catalyst and the substrate in the transition state, and at least one of those interactions must be stabilizing. Based on this model, in general one would expect that an associate pathway is a better mechanism for the enantioselectivity, and the three points are one steric interaction and two bonding interactions. To understand why path I, a stepwise path, has very good enantioselectivity, we show the transition-states structures (TS 11-1-*R* and TS 11-1-*S*) for hydride transfer in Figure 8. Interestingly, we found that both transition states have a strong hydrogen bond between N–H of iminium and oxygen of the coordinated CF_3COO^- ,

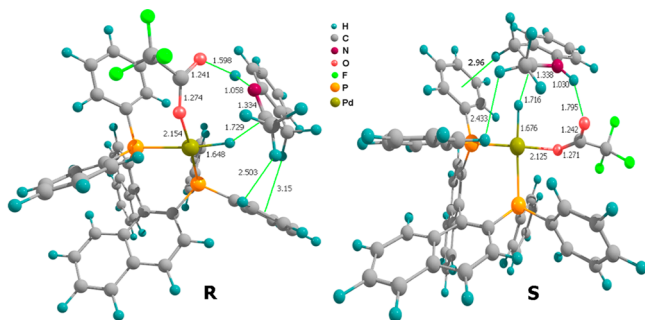


Figure 8. Computed structures of TS 11-1 (*R* and *S*). Bond lengths are given in Å.

and there is actually an eight-membered-ring transition state. Therefore, these transition states obey the “three-point interaction model”: the N–H...O hydrogen bond, the Pd...H...C bond, and the steric interaction between the ligand and the substrate. As shown in Figure 8, the steric interactions come mainly from CH_3 of the substrate and H(Ph) of the chiral ligand ($r_{\text{H}\cdots\text{H}} = 2.50$ Å in TS 11-1-*R* and 2.43 Å in TS 11-1-*S*), as well as CH_2 of the substrate and Ph of the chiral ligand (the distance between H(CH_2) and center of Ph is 3.15 Å for TS 11-1-*R* and 2.96 Å for TS 11-1-*S*). We do see a larger steric interaction for TS 11-1-*S*. In summary, despite the bond interaction and the steric interaction that exist for common stepwise mechanisms, here the hydrogen bond acts as the third point, and is expected to be crucial for the high enantioselectivity. This deduction is also demonstrated by the results of hydrogenation of *N*-protected indoles, in which either low activity or poor enantioselectivity was obtained due to the absence of the hydrogen bond between N–H of iminium and oxygen of coordinated trifluoroacetate (Scheme 3).

Paths II and III feature associated hydrogenation, which is usually thought to be found only for asymmetric reactions. The protonation costs 10.1 kcal/mol for path II and -3.5 kcal/mol for path III. The rate-determining steps for paths II and III are the associated hydrogenation steps, with the barrier of 59.2 kcal/mol (relative to **10**) for path II and 57.9 kcal/mol (relative to INT 13a) for path III (transition-state structures are shown in Figures 9 and 10). Our calculations suggest that both

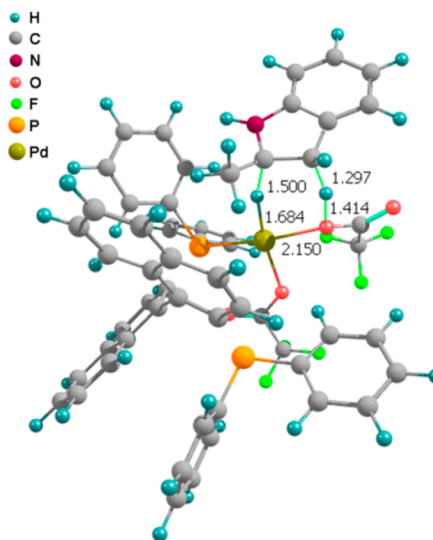


Figure 9. Computed structure of TS 12. Bond lengths are given in Å.

associated pathways degraded to stepwise pathways, where proton transfer to indole is followed by hydride transfer to iminium. Compared with path I, the hydride transfer is the same, while the proton transfer is not competitive because indole is more easily protonated (costs -5.8 kcal/mol) than the coordinated CF_3COO^- . For path IV, the barrier for Pd–H addition is 25.0 kcal/mol. However, the following proton transfer is much more difficult (energy barrier is 47.0 kcal/mol relative to **10**); therefore, this pathway is not preferred.

Generally, Pd-catalyzed asymmetric hydrogenation includes some important features: (1) Activation of hydrogen gas is a heterolytic process assisted by coordinated trifluoroacetate. (2) This is an ionic hydrogenation process. The hydride is from the hydrogen gas, while the proton is from a Brønsted acid. (3)

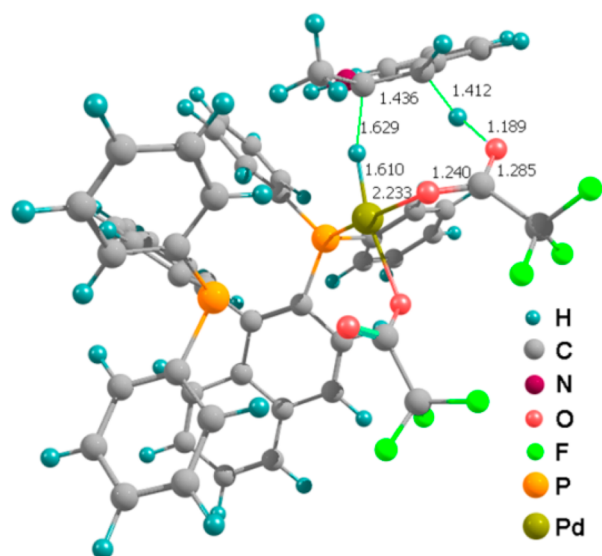


Figure 10. Computed structure of TS 13. Bond lengths are given in Å.

The mechanism is an outer-sphere hydrogenation mechanism. (4) The catalyst is bifunctional, leading to asymmetric hydrogenation and hydrogen-bonding interaction between trifluoroacetate of the Pd catalyst and iminium salt in the eight-membered-ring transition state for hydride transfer. (5) The highly polar solvent TFE stabilizes the ionic intermediates in active Pd–H species generation.

CONCLUSION

In conclusion, we report an extensive substrate scope for asymmetric hydrogenation of indoles, including 2-substituted and 2,3-disubstituted indoles. In this process, an equivalent of strong Brønsted acid was necessary to complete the reaction, giving up to 98% ee. This methodology was also applied in product elaboration for the synthesis of the biologically active indoline skeleton. Notably, a drawback is the low activity and/or enantioselectivity obtained for the 2-aryl-substituted and electron-withdrawing group located at the 2-position of the indoles. Given the compatibility of a Pd catalyst in this reaction, we also probed the properties of the Pd catalyst and the mechanism of indole hydrogenation by combining experimental studies and DFT calculations. Iminium salt was demonstrated to be the significant active intermediate in this reaction through the isotope-labeled reactions and ESI-HRMS. The strong acid protonates the C=C double bond of indole much easier, and therefore can remarkably decrease the energy barrier. According to the ^1H NMR spectrum of the Pd–H species, which was considered to be the active species, proton exchange between the Pd–H active species and solvent TFE could not occur. We have shown that in TFE the Pd–H active catalyst is generated by an ionic mechanism in which H_2 was split by Pd and trifluoroacetate via a six-membered-ring transition state. The reaction is only facile at room temperature with the help of the strong Brønsted acid. Highly polar solvent such as TFE is able to stabilize the ionic intermediates, making it better than the other solvents. We also propose that the Pd-catalyzed indole hydrogenation of unprotected indoles undergoes a stepwise, ionic, and outer-sphere hydrogenation mechanism,^{20,21} which features protonation of indole by a strong Brønsted acid and hydride transfer from active Pd–H to a protonated indole intermediate. The high enantioselectivity

observed experimentally was reproduced by the calculation, and is proposed to arise from the hydrogen-bonding interaction between N–H of iminium salt and oxygen of the coordinated trifluoroacetate ligand in the eight-membered-ring transition state for hydride transfer. So, active chiral Pd complex is a typical bifunctional catalyst, leading to asymmetric hydrogenation and hydrogen-bonding interaction between coordinated trifluoroacetate ligand of Pd catalyst and N–H of iminium salt. The above mechanistic study may provide some useful hints for chiral catalysis design and extend the scope of Pd-catalyzed asymmetric hydrogenation.

ASSOCIATED CONTENT

Supporting Information

Complete experimental procedures and characterization data for the prepared compounds. This material is available free of charge via the Internet at <http://pubs.acs.org>.

AUTHOR INFORMATION

Corresponding Authors

fanhj@dicp.ac.cn

ygzhou@dicp.ac.cn

Author Contributions

[†]Y.D. and L.L. contributed equally.

Notes

The authors declare no competing financial interest.

ACKNOWLEDGMENTS

This work was supported by National Natural Science Foundation of China (21125208, 21032003) and National Basic Research Program of China (2010CB833300). This paper is dedicated to Prof. Li-Xin Dai on the occasion of his 90th birthday.

REFERENCES

- (1) (a) Southon, I. W.; Buckingham, J. *Dictionary of Alkaloids*; Chapman and Hall: New York, 1989. (b) Neuss, N.; Neuss, M. N. In *The Alkaloids*; Brossi, A., Suffness, M., Eds.; Academic Press: San Diego, 1990; p 229. (c) Gueritte, F.; Fahy, J. In *Anticancer Agents from Natural Products*; Cragg, G. M., Kingstom, D. G. I., Newman, D. J., Eds.; CRC Press: Boca Raton, FL, 2005; p 123. (d) *Modern Alkaloids*; Fattorusso, E., Tagliatalata-Scafati, O., Eds.; Wiley-VCH: Weinheim, 2008, and references therein.
- (2) For recent reviews on asymmetric hydrogenation of aromatic compounds, see: (a) Zhao, D.; Glorius, F. *Angew. Chem., Int. Ed.* **2013**, *52*, 9616. (b) Wang, D.-S.; Chen, Q.-A.; Lu, S.-M.; Zhou, Y.-G. *Chem. Rev.* **2012**, *112*, 2557. (c) Tang, W.; Zhang, X. *Chem. Rev.* **2003**, *103*, 3029. (d) Kuwano, R. *Heterocycles* **2008**, *76*, 909. (e) Zhou, Y.-G. *Acc. Chem. Res.* **2007**, *40*, 1357. (f) Lu, S.-M.; Han, X.-W.; Zhou, Y.-G. *Chin. J. Org. Chem.* **2005**, *25*, 634. (g) Glorius, F. *Org. Biomol. Chem.* **2005**, *3*, 4171. For recent examples, see: (h) Ye, Z.-S.; Guo, R.-N.; Cai, X.-F.; Chen, M.-W.; Shi, L.; Zhou, Y.-G. *Angew. Chem., Int. Ed.* **2013**, *52*, 3685. (i) Iimuro, A.; Yamaji, K.; Kandula, S.; Nagano, T.; Kita, Y.; Mashima, K. *Angew. Chem., Int. Ed.* **2013**, *52*, 2046. (j) Ye, Z.-S.; Chen, M.-W.; Chen, Q.-A.; Shi, L.; Duan, Y.; Zhou, Y.-G. *Angew. Chem., Int. Ed.* **2012**, *51*, 10181. (k) Urban, S.; Beiring, B.; Ortega, N.; Paul, D.; Glorius, F. *J. Am. Chem. Soc.* **2012**, *134*, 15241. (l) Kuwano, R.; Morioka, R.; Kashiwabara, M.; Kameyama, N. *Angew. Chem., Int. Ed.* **2012**, *51*, 4136. (m) Shi, L.; Ye, Z.-S.; Cao, L.-L.; Guo, R.-N.; Hu, Y.; Zhou, Y.-G. *Angew. Chem., Int. Ed.* **2012**, *51*, 8286. (n) Wang, T.; Zhuo, L.-G.; Li, Z. W.; Chen, F.; Ding, Z.; He, Y.; Fan, Q.-H.; Xiang, J.; Yu, Z.-X.; Chan, A. S. C. *J. Am. Chem. Soc.* **2011**, *133*, 9878. (o) Urban, S.; Ortega, N.; Glorius, F. *Angew. Chem., Int. Ed.* **2011**, *50*, 3803. (p) Ortega, N.; Urban, S.; Beiring, B.; Glorius, F. *Angew. Chem.,*

- Int. Ed.* **2012**, *51*, 1710. (q) Ortega, N.; Tang, D.-T. D.; Urban, S.; Zhao, D.; Glorius, F. *Angew. Chem., Int. Ed.* **2013**, *52*, 9500.
- (3) (a) Kuwano, R.; Sato, K.; Kurokawa, T.; Karube, D.; Ito, Y. *J. Am. Chem. Soc.* **2000**, *122*, 7614. (b) Kuwano, R.; Kashiwabara, M.; Sato, K.; Ito, T.; Kaneda, K.; Ito, Y. *Tetrahedron: Asymmetry* **2006**, *17*, 521.
- (4) Kuwano, R.; Kaneda, K.; Ito, T.; Sato, K.; Kurokawa, T.; Ito, Y. *Org. Lett.* **2004**, *6*, 2213.
- (5) Kuwano, R.; Kashiwabara, M. *Org. Lett.* **2006**, *8*, 2653.
- (6) Mrcic, N.; Jerphagnon, T.; Minnaard, A. J.; Feringa, B. L.; de Vries, J. G. *Tetrahedron: Asymmetry* **2010**, *21*, 7.
- (7) Maj, A. M.; Suisse, I.; Meliet, C.; Agbossou-Niedercorn, F. *Tetrahedron: Asymmetry* **2010**, *21*, 2010.
- (8) Baeza, A.; Pfaltz, A. *Chem.—Eur. J.* **2010**, *16*, 2036.
- (9) Wang, D.-S.; Chen, Q.-A.; Li, W.; Yu, C.-B.; Zhou, Y.-G.; Zhang, X. *J. Am. Chem. Soc.* **2010**, *132*, 8909.
- (10) Wang, D.-S.; Tang, J.; Zhou, Y.-G.; Chen, M.-W.; Yu, C.-B.; Duan, Y.; Jiang, G.-F. *Chem. Sci.* **2011**, *2*, 803.
- (11) Duan, Y.; Chen, M.-W.; Ye, Z.-S.; Wang, D.-S.; Chen, Q.-A.; Zhou, Y.-G. *Chem.—Eur. J.* **2011**, *17*, 7193.
- (12) Duan, Y.; Chen, M.-W.; Chen, Q.-A.; Yu, C.-B.; Zhou, Y.-G. *Org. Biomol. Chem.* **2012**, *10*, 1235.
- (13) Recently, Chen and co-workers developed an asymmetric hydrosilylation of indoles, using combined Lewis base along with Brønsted acid activation to ensure full conversion and high enantioselectivity: Xiao, Y.-C.; Wang, C.; Yao, Y.; Sun, J.; Chen, Y.-C. *Angew. Chem., Int. Ed.* **2011**, *50*, 10661.
- (14) Chen, Q.-A.; Ye, Z.-S.; Duan, Y.; Zhou, Y.-G. *Chem. Soc. Rev.* **2013**, *42*, 497.
- (15) (a) Abe, H.; Amii, H.; Uneyama, K. *Org. Lett.* **2001**, *3*, 313. (b) Suzuki, A.; Mae, M.; Amii, H.; Uneyama, K. *J. Org. Chem.* **2004**, *69*, 5132. (c) Wang, Y.-Q.; Zhou, Y.-G. *Synlett* **2006**, 1189. (d) Yang, Q.; Shang, G.; Gao, W.; Deng, J.; Zhang, X. *Angew. Chem., Int. Ed.* **2006**, *45*, 3832. (e) Wang, Y.-Q.; Lu, S.-M.; Zhou, Y.-G. *J. Org. Chem.* **2007**, *72*, 3729. (f) Wang, Y.-Q.; Yu, C.-B.; Wang, D.-W.; Wang, X.-B.; Zhou, Y.-G. *Org. Lett.* **2008**, *10*, 2071. (g) Yu, C.-B.; Wang, D.-W.; Zhou, Y.-G. *J. Org. Chem.* **2009**, *74*, 5633. (h) Chen, M.-W.; Duan, Y.; Chen, Q.-A.; Wang, D.-S.; Yu, C.-B.; Zhou, Y.-G. *Org. Lett.* **2010**, *12*, 5075. (i) Zhou, X.-Y.; Bao, M.; Zhou, Y.-G. *Adv. Synth. Catal.* **2011**, *353*, 84. (j) McLaughlin, M.; Belyk, K.; Chen, C.-Y.; Linghu, X.; Pan, J.; Qian, G.; Reamer, R. A.; Xu, Y. *Org. Process Res. Dev.* **2013**, *17*, 1052.
- (16) (a) Yu, C.-B.; Gao, K.; Wang, D.-S.; Shi, L.; Zhou, Y.-G. *Chem. Commun.* **2011**, 47, 5052. (b) Yu, C.-B.; Gao, K.; Chen, Q.-A.; Chen, M.-W.; Zhou, Y.-G. *Tetrahedron Lett.* **2012**, *53*, 2560.
- (17) (a) Raja, R.; Thomas, J. M.; Jones, M. D.; Johnson, B. F. G.; Vaughan, D. E. W. *J. Am. Chem. Soc.* **2003**, *125*, 14982. (b) Wang, Y.-Q.; Lu, S.-M.; Zhou, Y.-G. *Org. Lett.* **2005**, *7*, 3235. (c) Goulioukina, N. S.; Bondarenko, G. N.; Bogdanov, A. V.; Gavrilov, K. N.; Beletskaya, I. P. *Eur. J. Org. Chem.* **2009**, 510. (d) Wang, C.; Yang, G.; Zhuang, J.; Zhang, W. *Tetrahedron Lett.* **2010**, *51*, 2044. (e) Teng, B.; Zheng, J.; Huang, H.; Huang, P. *Chin. J. Chem.* **2011**, *29*, 1312. (f) Zhou, X.-Y.; Wang, D.-S.; Bao, M.; Zhou, Y.-G. *Tetrahedron Lett.* **2011**, *52*, 2826.
- (18) (a) Drago, D.; Pregosin, P. S. *Organometallics* **2002**, *21*, 1208. (b) Jones, M. D.; Raja, R.; Thomas, J. M.; Johnson, B. F. G.; Lewis, D. W.; Rouzaud, J.; Harris, K. D. M. *Angew. Chem., Int. Ed.* **2003**, *42*, 4326. (c) Tsuchiya, Y.; Hamashima, Y.; Sodeoka, M. *Org. Lett.* **2006**, *8*, 4851. (d) Monguchi, D.; Beemelmans, C.; Hashizume, D.; Hamashima, Y.; Sodeoka, M. *J. Organomet. Chem.* **2008**, *693*, 867. (e) Arnanz, A.; González-Arellano, C.; Juan, A.; Villaverde, G.; Corma, A.; Iglesias, M.; Sánchez, F. *Chem. Commun.* **2010**, 46, 3001. (f) Boronat, M.; Corma, A.; González-Arellano, C.; Iglesias, M.; Sánchez, F. *Organometallics* **2010**, *29*, 134. (g) Wang, D.-S.; Wang, D.-W.; Zhou, Y.-G. *Synlett* **2011**, 947.
- (19) (a) Wang, D.-S.; Ye, Z.-S.; Chen, Q.-A.; Zhou, Y.-G.; Yu, C.-B.; Fan, H.-J.; Duan, Y. *J. Am. Chem. Soc.* **2011**, *133*, 8866. (b) Li, C.; Chen, J.; Fu, G.; Liu, D.; Liu, Y.; Zhang, W. *Tetrahedron* **2013**, *69*, 6839.
- (20) (a) Zhu, Y.; Burgess, K. *Acc. Chem. Res.* **2012**, *45*, 1623. (b) Zhou, J.; Ogle, J. W.; Fan, Y.; Banphavichit, V.; Zhu, Y.; Burgess, K. *Chem.—Eur. J.* **2007**, *13*, 7162. (c) Perry, M. C.; Cui, X. H.; Powell, M. T.; Hou, D. R.; Reibenspies, J. H.; Burgess, K. *J. Am. Chem. Soc.* **2003**, *125*, 113. (d) O, W. W. N.; Lough, A. J.; Morris, R. H. *Organometallics* **2012**, *31*, 2152. (e) Maeda, T.; Makino, K.; Iwasaki, M.; Hamada, Y. *Chem.—Eur. J.* **2010**, *16*, 11954. (f) Hopmann, K. H.; Bayer, A. *Organometallics* **2011**, *30*, 2483. (g) Fan, Y. B.; Cui, X. H.; Burgess, K.; Hall, M. B. *J. Am. Chem. Soc.* **2004**, *126*, 16688. (h) Dobereiner, G. E.; Nova, A.; Schley, N. D.; Hazari, N.; Miller, S. J.; Eisenstein, O.; Crabtree, R. H. *J. Am. Chem. Soc.* **2011**, *133*, 7547.
- (21) (a) Sandoval, C. A.; Ohkuma, T.; Utsumi, N.; Tsutsumi, K.; Murata, K.; Noyori, R. *Chem.—Asian J.* **2006**, *1*, 102. (b) Sandoval, C. A.; Ohkuma, T.; Muniz, K.; Noyori, R. *J. Am. Chem. Soc.* **2003**, *125*, 13490. (c) Phillips, S. D.; Fuentes, J. A.; Clarke, M. L. *Chem.—Eur. J.* **2010**, *16*, 8002. (d) Kitamura, M.; Tsukamoto, M.; Bessho, Y.; Yoshimura, M.; Kobs, U.; Widhalm, M.; Noyori, R. *J. Am. Chem. Soc.* **2002**, *124*, 6649. (e) Girard, C.; Genet, J. P.; Bulliard, M. *Eur. J. Org. Chem.* **1999**, 2937. (f) Ashby, M. T.; Halpern, J. *J. Am. Chem. Soc.* **1991**, *113*, 589.
- (22) (a) Roucoux, A.; Thieffry, L.; Carpentier, J. F.; Devocelle, M.; Meliet, C.; Agbossou, F.; Mortreux, A. *Organometallics* **1996**, *15*, 2440. (b) Kless, A.; Borner, A.; Heller, D.; Selke, R. *Organometallics* **1997**, *16*, 2096. (c) Imamoto, T.; Tamura, K.; Zhang, Z.; Horiuchi, Y.; Sugiya, M.; Yoshida, K.; Yanagisawa, A.; Gridnev, I. D. *J. Am. Chem. Soc.* **2012**, *134*, 1754. (d) Heller, D.; Kadyrov, R.; Michalik, M.; Freier, T.; Schmidt, U.; Krause, H. W. *Tetrahedron: Asymmetry* **1996**, *7*, 3025. (e) Haag, D.; Runsink, J.; Scharf, H. D. *Organometallics* **1998**, *17*, 398. (f) Gridnev, I. D.; Imamoto, T.; Hoge, G.; Kouchi, M.; Takahashi, H. *J. Am. Chem. Soc.* **2008**, *130*, 2560. (g) Gridnev, I. D.; Higashi, N.; Asakura, K.; Imamoto, T. *J. Am. Chem. Soc.* **2000**, *122*, 7183. (h) Fabrello, A.; Bachelier, A.; Urrutigoity, M.; Kalck, P. *Coord. Chem. Rev.* **2010**, *254*, 273.
- (23) (a) Ettel, V.; Myska, J. *Chem. Abstr.* **1956**, 5619. (b) Ettel, V.; Myska, J. *Collect. Czech. Chem. Commun.* **1956**, *21*, 473. (c) Zhao, H.; He, X. S.; Thurkauf, A.; Hoffman, D.; Kietlyka, A.; Brodbeck, R.; Primus, R.; Wasley, J. W. F. *Bioorg. Med. Chem. Lett.* **2002**, *12*, 3111. (d) Zhao, H.; Thurkauf, A.; He, X. S.; Hodgetts, K.; Zhang, X. Y.; Rachwal, S.; Kover, R. X.; Hutchison, A.; Peterson, J.; Kietlyka, A.; Brodbeck, R.; Primus, R.; Wasley, J. W. F. *Bioorg. Med. Chem. Lett.* **2002**, *12*, 3105.
- (24) (a) Chen, C.-B.; Wang, X.-F.; Cao, Y.-J.; Cheng, H.-G.; Xiao, W.-J. *J. Org. Chem.* **2009**, *74*, 3532. (b) Hinman, R. L.; Shull, E. R. *J. Org. Chem.* **1961**, *26*, 2339. (c) Ballini, R.; Palmieri, A.; Petrini, M.; Shaikha, R. R. *Adv. Synth. Catal.* **2008**, *350*, 129. (d) Li, Y.; Shi, F.-Q.; He, Q.-L.; You, S.-L. *Org. Lett.* **2009**, *11*, 3182. (e) Zheng, B.-H.; Ding, C.-H.; Hou, X.-L.; Dai, L.-X. *Org. Lett.* **2010**, *12*, 1688. (f) Jing, L.; Wei, J.; Zhou, L.; Huang, Z.; Li, Z.; Wu, D.; Xiang, H.; Zhou, X. *Chem.—Eur. J.* **2010**, *16*, 10955.
- (25) (a) Grushin, V. V. *Chem. Rev.* **1996**, *96*, 2011. (b) Hills, I. D.; Fu, G. C. *J. Am. Chem. Soc.* **2004**, *126*, 13178. (c) Konnick, M. M.; Gandhi, B. A.; Guzei, I. A.; Stahl, S. S. *Angew. Chem., Int. Ed.* **2006**, *45*, 2904. (d) Nielsen, R. J.; Goddard, W. A. *J. Am. Chem. Soc.* **2006**, *128*, 9651. (e) Popp, B. V.; Stahl, S. S. *J. Am. Chem. Soc.* **2007**, *129*, 4410. (f) Konnick, M. M.; Stahl, S. S. *J. Am. Chem. Soc.* **2008**, *130*, 5753. (g) Popp, B. V.; Stahl, S. S. *Chem.—Eur. J.* **2009**, *15*, 2915. (h) Decharin, N.; Stahl, S. S. *J. Am. Chem. Soc.* **2011**, *133*, 5732. (i) Sigman, M. S.; Jensen, D. R. *Acc. Chem. Res.* **2006**, *39*, 221. (j) Gligorich, K. M.; Schultz, M. J.; Sigman, M. S. *J. Am. Chem. Soc.* **2006**, *128*, 2794. (k) Schultz, M. J.; Adler, R. S.; Zierkiewicz, W.; Privalov, T.; Sigman, M. S. *J. Am. Chem. Soc.* **2005**, *127*, 8499.
- (26) (a) Leoni, P.; Sommovigo, M.; Pasquali, M.; Midollini, S.; Braga, D.; Sabatino, P. *Organometallics* **1991**, *10*, 1038. (b) Portnoy, M.; Frolow, F.; Milstein, D. *Organometallics* **1991**, *10*, 3960. (c) Leoni, P.; Pasquali, M.; Sommovigo, M.; Laschi, F.; Zanello, P.; Albinati, A.; Lianza, F.; Pregosin, P. S.; Rueegger, H. *Organometallics* **1993**, *12*, 1702. (d) Portnoy, M.; Milstein, D. *Organometallics* **1994**, *13*, 600. (e) Fantasia, S.; Egbert, J. D.; Jurčik, V.; Cazin, C. S. J.; Jacobsen, H.; Cavallo, L.; Heinekey, D. M.; Nolan, S. P. *Angew. Chem., Int. Ed.* **2009**,

48, 5182. (f) Fulmer, G. R.; Muller, R. P.; Kemp, R. A.; Goldberg, K. I. *J. Am. Chem. Soc.* **2009**, *131*, 1346. (g) Fulmer, G. R.; Herndon, A. N.; Kaminsky, W.; Kemp, R. A.; Goldberg, K. I. *J. Am. Chem. Soc.* **2011**, *133*, 17713. (h) Vyas, D. J.; Larionov, E.; Besnard, C.; Guénee, L.; Mazet, C. *J. Am. Chem. Soc.* **2013**, *135*, 6830.

(27) All calculations were carried out using Density Functional Theory as implemented in the Jaguar 7.5 suite of ab initio quantum chemistry programs. Geometry optimizations were performed with the B3LYP functional and the 6-31G** basis set with no symmetry restrictions. Palladium was represented using the Los Alamos LACVP basis. Solvation energies were evaluated by a self-consistent reaction field (SCRF) approach based on accurate numerical solutions of the Poisson–Boltzmann equation. The free energy in solution phase was calculated as $G(\text{sol}) = E(\text{SCF}) + \text{ZPE} - \text{TS}(\text{gas}) + G^{\text{solv}}$.

(28) Fey, N.; Ridgway, B. M.; Jover, J.; McMullin, C. L.; Harvey, J. N. *Dalton Trans.* **2011**, *40*, 11184.

(29) (a) Bonnet-Delpon, D.; Bégué, J.-P.; Crousse, B. *Synlett* **2004**, 18. (b) Börner, A.; Shuklov, I.; Dubrovina, N. *Synthesis* **2007**, *2007*, 2925.

(30) (a) Ebersson, L.; Hartshorn, M. P.; Persson, O.; Radner, F. *Chem. Commun.* **1996**, 2105. (b) Munshi, P.; Main, A. D.; Linehan, J. C.; Tai, C.-C.; Jessop, P. G. *J. Am. Chem. Soc.* **2002**, *124*, 7963.

(31) (a) Guari, Y.; Ayllon, J. A.; Sabo-Etienne, S.; Chaudret, B.; Hessen, B. *Inorg. Chem.* **1998**, *37*, 640. (b) Fache, F.; Piva, O. *Synlett* **2004**, 1294. (c) Ng, S. M.; Yin, C.; Yeung, C. H.; Chan, T. C.; Lau, C. P. *Eur. J. Inorg. Chem.* **2004**, *2004*, 1788. (d) Vuluga, D.; Legros, J.; Crousse, B.; Slawin, A. M. Z.; Laurence, C.; Nicolet, P.; Bonnet-Delpon, D. *J. Org. Chem.* **2011**, *76*, 1126.

(32) (a) Teunissen, H. T. *Chem. Commun.* **1998**, 1367. (b) Bakhmutova, E. V.; Bakhmutov, V. I.; Belkova, N. V.; Besora, M.; Epstein, L. M.; Lledos, A.; Nikonov, G. I.; Shubina, E. S.; Tomas, J.; Vorontsov, E. V. *Chem.—Eur. J.* **2004**, *10*, 661. (c) Donghi, D.; Beringhelli, T.; D'Alfonso, G.; Mondini, M. *Chem.—Eur. J.* **2006**, *12*, 1016. (d) Dub, P. A.; Fillipov, O. A.; Silant'ev, G. A.; Belkova, N. V.; Daran, J.-C.; Epstein, L. M.; Poli, R.; Shubina, E. S. *Eur. J. Inorg. Chem.* **2010**, 1489.

(33) (a) Easson, L. H.; Stedman, E. J. *Biochem.* **1933**, *27*, 1257. (b) Simón, L.; Goodman, J. M. *J. Am. Chem. Soc.* **2008**, *130*, 8741.